CrossMark

# Drafting, kissing and tumbling process of two particles with different sizes

L. Wang [a,b], Z.L. Guo [b,*], J.C. Mi [a]

[a] State Key Laboratory of Turbulence and Complex Systems, College of Engineering, Peking University, Beijing 100871, China
[b] State Key Laboratory of Coal Combustion, Huazhong University of Science and Technology, Wuhan 430074, Hubei, China

A B S T R A C T

We numerically study the drafting, kissing and tumbling (DKT) phenomenon of two non-identical circular particles sedimenting in a two-dimensional infinite channel by using the lattice Boltzmann equation with a multiple-relaxation-time collision model. The main emphasis of this work is to investigate the effect of the longitudinal distance and diameter ratio between two particles on the flow pattern during sedimentation. The method is first validated by simulating the sedimentation of one single particle and two identical particles. For two particles with different sizes, two cases are considered: in Case-1, the larger particle is initially located above the smaller one; in Case-2, the smaller particle is initially above the larger one. The simulation results are compared with the case of two equal-sized particles. The results show that two particles with different sizes are easier to separate than two identical ones. In particular, the effects of initial longitudinal distance ($D_h$) and diameter ratio on the occurrence of the DKT process are studied in detail. With changing these two parameters, the results reveal the transitions between the DKT phenomena. It is shown that the DKT process can take place (only once) regardless of any value of $D_h$ in Case-1, while in Case-2, the two particles will never undergo the DKT process when increasing $D_h$ beyond a certain threshold. The results also show that, as the particle diameter ratio $\gamma$ is increased starting from 1, in Case-1 the two particles will interact by undergoing two transitions of the DKT phenomena: from the repeated to the one-off DKT process, while in Case-2 there exists an additional mode: the gap increases continuously from the start.

© 2014 Elsevier Ltd. All rights reserved.

## 1. Introduction

Sedimentation of particles in a viscous fluid occurs in a variety of natural and industrial applications, such as fluidization, the petroleum and paper industries, and blood flows. This subject has attracted much attention in theoretical and experimental studies for many years, and a variety of numerical methods have been developed and used to study particle–fluid systems.

As an alternative computational approach for the Navier–Stokes (NS) equations, the lattice-Boltzmann method (LBM) [1–5] has also been shown to be an effective tool for simulating particulate suspensions. In this method, the fluid behavior is described by a mesoscopic model based on the discrete Boltzmann equation which is marched explicitly in time according to simple rules. It has been shown that through a multi-scaling analysis, the NS equations can be recovered. The application of LBM to particle–fluid suspensions was first presented by Ladd [1,2], who proposed a

modified bounce-back rule to account for the boundary velocity of a moving particle. The flow field and the solid particle are represented by a fixed uniform grid system, and the hydrodynamic force and torque on the particle are calculated based on a simple momentum exchange method, whose motion and rotation are determined by the Newtonian dynamics. This method provides a fast and efficient simulation of solid–fluid suspension flow. Since then, the LBM has become a popular tool for simulating particulate flows [6–10].

In particulate flows, fundamental mechanisms of fluid-particle and particle–particle interactions are very important for accurately predicting the flow behaviors. The sedimentation of two circular particles serves as the simplest problem to study these two types of interactions, and many experimental and numerical studies have been carried out to investigate the behavior of sedimentation of circular particles. Fortes et al. [11] observed experimentally that in the sedimentation of two particles in a Newtonian fluid inside a vertical channel, the two particles would undergo the drafting, kissing and tumbling (DKT) phenomenon. Theoretical investigation of hydrodynamic interactions between two particles can be found

in Refs. [12,13]. Based on a finite element method (FEM), Feng et al. [14] simulated the motion of circular particles sedimenting in a vertical channel and successfully predicted the DKT phenomenon. They also analyzed the fluid-particle, particle–wall and particle–particle interactions. With a finite volume method, Ritz and Caltagirone [15] numerically simulated the motion of settling particles in two dimensions and also predicted the DKT phenomenon. Some modifications of the distributed Lagrange multiplier-based fictitious domain method (DLM) for dynamical simulation of fluid-particle suspensions can also be found in the literatures [16–18]. Using the LBM, earlier attempts to simulate the sedimentation of two circular particles had fully reproduced the DKT process [5], where the motion of solid particles were succinctly analyzed. Recently, a number of hybrid methods have been developed in which the LBM is coupled with other methods, such as the immersed boundary method (IBM) [9], Discrete Element Method [19], and FEM [20] to simulate particle suspensions.

The sedimentation process of two particles is significantly influenced by a number of intrinsic factors, such as particle density, shape and surface properties. But in most cases, the particle size and density plays the dominant role in the real engineering applications. So far, most of numerical studies of interactions between two sedimenting particles concentrate on uniform particle sizes. The attention paid to the effect of diameter ratio on particle motion and interactions is very limited. Mukundakrishnan et al. [21] numerically investigated the motion of two particles in a finite fluid-filled rotating cylinder. They also considered the particle size and density effect on the flow behaviors. Shao et al. [22] simulated the sedimentation of two circular particles with different sizes using the DLM/Fictitious Domain method. The effect of diameter ratio on the interaction of two sedimenting circular particles was studied. They discovered that for small diameter ratio (below 1.111), the two particles would undergo the DKT process repeatedly and the frequency increased as the diameter ratio decreased, while enlarging the diameter ratio to some values, the two particles would separate after their tumbling. In addition, they found that the influence of interactions on the motion of the small particle was more stronger than that of the large particle. However, it is noticed that their analysis was restricted to a fixed configuration in the channel, and the study is not enough to reveal the mechanism of the interactions of two sedimenting particles with different sizes. A more detailed study on the effect of diameter ratio would be required. To our knowledge, few attention have been paid to this issue. Therefore, the main focus of our present effort is to investigate the effects of size ratio on the sedimentation of two circular particles. In this paper, we will conduct a systemic investigation on this problem by using the LBM. We intend to understand the mechanisms for the behavior of two particles induced by the fluid-particle and particle–particle interactions together with the particle–wall interactions by considering the difference in size and initial position of the particles.

Up to now, the lattice Bhatnagar-Gross-Krook (LBGK) model is the most popular LBM used in particulate flows for its simplicity. However, this model has some shortcomings. For instance, the BGK model may suffer from numerical instability when simulating fluids with relatively low viscosities [23–25]. In view of the defect inherent in the BGK model, the multiple-relaxation-time (MRT) model [23,24,26] has been proposed recently to simulate particulate flows [27–29]. More importantly, the MRT model can achieve better accuracy and robustness than the BGK model in particulate flows [29]. Therefore, the present numerical simulations are conducted with the MRT model. The rest of the paper is organized as follows. Section 2 gives a brief review of the MRT LB model. The code is first validated by comparing the present results with the existing results for the sedimentation of two identical particles in an infinite channel in Section 3. With reference to the results of

two identical particles, the effect of size ratio and initial longitudinal distance between two non-identical particles on their interactions are subsequently studied at two types of initial configurations. Finally, some concluding remarks are presented in Section 4.

## 2. Numerical method

So far, the LBM has been well-documented for simulations of particles suspended in fluid, and many variants of this method can be found in the review paper [8]. In this section, we will provide a brief overview of two-dimensional MRT lattice Boltzmann equation (LBE) model used in our simulations.

### 2.1. Multiple-relaxation-time lattice Boltzmann method

For the two-dimensional MRT model with nine velocities (D2Q9 model), the evolution of MRT-LBE can be expressed as [23,24,26],

$$\boldsymbol{f}(\boldsymbol{x}_j + \boldsymbol{c}\delta_t, t + \delta_t) - \boldsymbol{f}(\boldsymbol{x}_j, t) = -\boldsymbol{M}^{-1}\boldsymbol{S}[\boldsymbol{m}(\boldsymbol{x}_j, t) - \boldsymbol{m}^{(eq)}(\boldsymbol{x}_j, t)], \quad (1)$$

where

$$\boldsymbol{f}(\boldsymbol{x}_j + \boldsymbol{c}\delta_t, t + \delta_t) = (f_0(\boldsymbol{x}_j, t + \delta_t), f_1(\boldsymbol{x}_j + \boldsymbol{c}_1\delta_t, t + \delta_t), \dots, f_8(\boldsymbol{x}_j + \boldsymbol{c}_8\delta_t, t + \delta_t))^T,$$

$$\boldsymbol{f}(\boldsymbol{x}_j, t) = (f_0(\boldsymbol{x}_j, t), f_1(\boldsymbol{x}_j, t), \dots, f_8(\boldsymbol{x}_j, t))^T$$

are 9-dimensional vectors of the discrete distribution functions $\{f_i | i = 0, 1, \dots, 8\}$, in which $f_i(\boldsymbol{x}_j, t)$ is the fluid distribution function for particle moving with discrete velocity $\boldsymbol{c}_i$ at time $t$ and position $\boldsymbol{x}_j$. $\boldsymbol{m}$ and $\boldsymbol{m}^{(eq)}$ are 9-dimensional vectors of velocity moments of the distribution functions $\boldsymbol{f}$ and their equilibria, respectively. $\boldsymbol{M}$ is a $9 \times 9$ matrix which linearly transforms the distribution functions to their moments,

$$\boldsymbol{m} = \boldsymbol{M} \cdot \boldsymbol{f}, \quad \boldsymbol{f} = \boldsymbol{M}^{-1} \cdot \boldsymbol{m},$$

and $\boldsymbol{S}$ is a non-negative $9 \times 9$ diagonal relaxation matrix. $\delta_t$ is the time step, and the discrete velocity set $\{\boldsymbol{c}_i | i = 0, 1, \dots, 8\}$ in the D2Q9 model is

$$\boldsymbol{c}_i = \begin{cases} (0, 0), & i = 0, \\ (\cos[(i-1)\pi/2], \sin[(i-1)\pi/2])c, & i = 1-4, \\ (\cos[(2i-1)\pi/4], \sin[(2i-1)\pi/4])\sqrt{2}c, & i = 5-8, \end{cases} \quad (2)$$

where $c = \delta x/\delta t$ is the lattice speed, and $\delta x$ is the lattice cell width.

Corresponding to the above nine-velocity LBE model, we can arrange the components of the moment vector in the following order:

$$\boldsymbol{m} = (\rho, e, \varepsilon, j_x, q_x, j_y, q_y, p_{xx}, p_{xy})^T,$$

where $\rho$ is the fluid density, $e$ and $\varepsilon$ are related to the total energy and the energy square, $j_x = \rho u_x$ and $j_y = \rho u_y$ are $x$ and $y$ components of the momentum, respectively; $q_x$ and $q_y$ are related to the $x$ and $y$ components of the energy flux, and $p_{xx}$ and $p_{xy}$ are the symmetric and traceless components of the stress tensor, respectively. The equilibrium moments of $\boldsymbol{m}$ can be written accordingly as

$$\boldsymbol{m}^{(eq)} = (\rho, e^{(eq)}, \varepsilon^{(eq)}, j_x, q_x^{(eq)}, j_y, q_y^{(eq)}, p_{xx}^{(eq)}, p_{xy}^{(eq)})^T, \quad (3)$$

where the density $\rho$ and the momentum $\boldsymbol{j} = \rho\boldsymbol{u}$ are the conserved moments. The equilibria of the non-conserved moments in (3) are functions of the conserved moments, which are defined by [23,24],

$$e^{(eq)} = \rho(-2 + 3u_x^2 + 3u_y^2), \quad (4a)$$

$$\varepsilon^{(eq)} = -\rho\left(-1 + 3u_x^2 + 3u_y^2\right), \quad (4b)$$

$$q_x^{(eq)} = -\rho u_x, \qquad q_y^{(eq)} = -\rho u_y, \quad (4c)$$

$$p_{xx}^{(eq)} = \rho(u_x^2 - u_y^2), \quad p_{xy}^{(eq)} = \rho u_x u_y. \quad (4d)$$

With the ordering of discrete velocities and moments specified above, the transformation matrix $\boldsymbol{M}$ is given by [23]

$$\boldsymbol{M} = \begin{pmatrix} 1 & 1 & 1 & 1 & 1 & 1 & 1 & 1 & 1 \\ -4 & -1 & -1 & -1 & -1 & 2 & 2 & 2 & 2 \\ 4 & -2 & -2 & -2 & -2 & 1 & 1 & 1 & 1 \\ 0 & 1 & 0 & -1 & 0 & 1 & -1 & -1 & 1 \\ 0 & -2 & 0 & 2 & 0 & 1 & -1 & -1 & 1 \\ 0 & 0 & 1 & 0 & -1 & 1 & 1 & -1 & -1 \\ 0 & 0 & -2 & 0 & 2 & 1 & 1 & -1 & -1 \\ 0 & 1 & -1 & 1 & -1 & 0 & 0 & 0 & 0 \\ 0 & 0 & 0 & 0 & 0 & 1 & -1 & 1 & -1 \end{pmatrix}. \tag{5}$$

Note that the mass and monmentum do not change before and after the collision. Therefore, the diagonal relaxation matrix is given by

$$\boldsymbol{S} = diag(0, s_1, s_2, 0, s_4, 0, s_5, s_6, s_7, s_8), \tag{6}$$

where the non-negative relaxation rates can affect the stability of the model [23,24], and must be be chosen in the range $0 < s_i < 2$ to satisfy the stability condition for non-conserved moments.

The density $\rho$ and velocity $\boldsymbol{u}$ of the fluid are determined by

$$\rho = \sum_i f_i, \qquad \rho\boldsymbol{u} = \sum_i \boldsymbol{c}_i f_i. \tag{7}$$

With the aid of the Chapman-Enskog expansion, the Navier–Stokes equations can be recovered from the LBE of (1) in the low Mach number limit, with the shear viscosity $v$ and the bulk viscosity $\zeta$ being given by

$$v = c_s^2 \left(\frac{1}{s_7} - \frac{1}{2}\right)\delta_t, \quad \zeta = c_s^2 \left(\frac{1}{s_1} - \frac{1}{2}\right)\delta_t. \tag{8}$$

where $c_s = c/\sqrt{3}$ is the speed of sound. In MRT model, $c$ is usually set to be unity. In addition, it is required that $s_7 = s_8$ and $s_4 = s_6$.

It should be noted that when all the relaxation rates equal to $1/\tau$, where $\tau$ is the relaxation time in BGK model, the MRT model will reduce to the BGK counterpart, of which the equilibrium distribution function (EDF) $f_j^{(eq)}(\boldsymbol{x}, t)$ are defined by the fluid density $\rho$ and velocity $\boldsymbol{u}$,

$$f_i^{(eq)} = \omega_i \rho \left[1 + \frac{\boldsymbol{c}_i \cdot \boldsymbol{u}}{c_s^2} + \frac{(\boldsymbol{c}_i \cdot \boldsymbol{u})^2}{2c_s^4} - \frac{\boldsymbol{u}^2}{2c_s^2}\right], \tag{9}$$

where $\omega_i$ is the weighting factor which is given by $\omega_0 = 4/9, \omega_{1-4} = 1/9, \omega_{5-8} = 1/36$, and the sound speed is $c_s = c/\sqrt{3}$. In this model, the fluid viscosity is computed by $v = c_s^2(\tau - 1/2)\delta_t$.

The evolution process of MRT-LBE consists of two steps, i.e., the collision step and the streaming one. The collision step is first executed in the moment space and then mapped to the velocity space,

$$\boldsymbol{m}^*(\boldsymbol{x}, t) = \boldsymbol{m}(\boldsymbol{x}, t) - \boldsymbol{S}\left[\boldsymbol{m}(\boldsymbol{x}, t) - \boldsymbol{m}^{(eq)}(\boldsymbol{x}, t)\right],$$
$$\boldsymbol{f}^*(\boldsymbol{x}, t) = \boldsymbol{M}^{-1}\boldsymbol{m}^*(\boldsymbol{x}, t). \tag{10}$$

while the streaming step is still implemented in velocity space,

$$f_i(\boldsymbol{x} + \boldsymbol{c}_i\delta_t, t + \delta_t) = f_i^*(\boldsymbol{x}, t). \tag{11}$$

### 2.2. Boundary conditions for fluid-particle interaction

In LBE for particulate flows, boundary conditions at the surface of a moving particle is an important topic, and some different schemes has been proposed in the literature. As one of the most notable contributions, Ladd [1] and Ladd and Verberg [8] developed an efficient and simple method to treat the boundary condition on the particle–fluid interface. In this method, a fixed regular grid system is used to represent the solid particle in addition to the flow field. The interior of the suspended particle is filled with the fluid, and the fluid can pass through its boundary. Such an assumption can bring facilitation to the computations since the fluid nodes both inside and outside the particle can be treated in the same manner as the particle moves on the meshes.

On the other hand, the surface of a particle in Ladd's method is represented by some boundary nodes defined as the midpoints between the neighboring fluid and solid nodes. This arrangement causes the real particle boundary to be replaced by a series of stairwise segments, which results in the distortion of the geometry and degrades the computational accuracy. One improvement on the representation of the particle boundary is to adopt the curved boundary condition [30]. Due to the uniform treatment for the boundary condition, we choose the interpolation scheme proposed by Yu et al. [31] for the curved boundary condition. In this interpolation scheme, the no-slip boundary on the particle surface is implemented by a bounce-back rule [1,8]:

$$f_{i'}(\boldsymbol{x}_b, t + \delta_t) = f_i^*(\boldsymbol{x}_b, t) - 2\omega_i \rho \frac{\boldsymbol{c}_i \cdot \boldsymbol{u}_b}{c_s^2}, \tag{12}$$

where $\boldsymbol{x}_b$ is the boundary node at the solid surface with velocity $\boldsymbol{u}_b$, $\boldsymbol{c}_{i'} = -\boldsymbol{c}_i$ denotes the reflection direction and $\boldsymbol{c}_i$ the incident direction. As in the method of Ladd, the inner of the particle is filled with the fluid as the particle moves, and the fluid can cross over the particle boundary.

As reported in some published works [32–34], through the bounce-back rule, the no-slip boundary condition is not always satisfied at one half nodes between the neighboring fluid and solid nodes. In the BGK model, the accurate boundary location depends on the fluid viscosity when the bounce-back is applied to the Poiseuille and Couette flows. While using the MRT-LBE model, this problem can be overcome by a proper choice of the relaxation parameters as the following [25,32]:

$$s_4 = s_6 = 8\frac{(2 - s_8)}{(8 - s_8)}, \tag{13}$$

and the no-slip boundary condition is satisfied at one half grid spacing of the last fluid node [35]. Therefore, we will follow this theoretical result to determine the relaxation rates in our simulations.

In LBE for simulations of particle suspensions, the calculation of the hydrodynamic force exerted on a solid particle is another important issue. The momentum-exchange method [1,6,36] and the stress-integration method [37,38] are two fundamental methods, and have been examined in the literature. In the following simulations, the momentum-exchange method will be chosen for its simplicity and accuracy. At each lattice node $\boldsymbol{x}_f$ nearest neighboring a boundary node $\boldsymbol{x}_b$, the force exerted by the fluid on the solid particle results from the momentum exchange (per unit time) between the incident direction $\boldsymbol{c}_i$ and the reflection direction $\boldsymbol{c}_{i'}$ of $\boldsymbol{x}_f$

$$F_i(\boldsymbol{x}_f, t) = \frac{\delta_x^2}{\delta_t}\left[\boldsymbol{c}_i f_i^*(\boldsymbol{x}_f, t) - \boldsymbol{c}_{i'} f_{i'}(\boldsymbol{x}_f, t + \delta_t)\right]. \tag{14}$$

After summing over all nearest lattice nodes neighboring all boundary nodes and all relevant directions for each boundary node, the total hydrodynamic force $\boldsymbol{F}_t$ and torque $\boldsymbol{T}_t$ on the solid particle can be obtained as

$$\boldsymbol{F}_t = \sum_{\boldsymbol{x}_f}\sum_i \boldsymbol{F}_i(\boldsymbol{x}_f), \quad \boldsymbol{T}_t = \sum_{\boldsymbol{x}_b, \boldsymbol{x}_f}\sum_i (\boldsymbol{x}_b - \boldsymbol{R}) \times \boldsymbol{F}_i(\boldsymbol{x}_f), \tag{15}$$

Once $\boldsymbol{F}_t$ and $\boldsymbol{T}_t$ on the solid particle are calculated, the translational velocity $\boldsymbol{u}_p$ and the angular velocity $\boldsymbol{\Omega}_p$ of the particle are determined by Newton's law as follows:

$$M_p \frac{d\boldsymbol{u}_p}{dt} = \boldsymbol{F}_t, \quad I_p \frac{d\boldsymbol{\Omega}_p}{dt} = \boldsymbol{T}_t, \tag{16}$$

where $M_p$ and $I_p$ are the mass and the moment inertia of the particle, respectively. For the numerical computations of these two equations, the first-order Euler method is executed in our simulations to update the translation and rotation of the particle at each time step:

$$\boldsymbol{u}_p^{n+1} = \boldsymbol{u}_p^n + \delta_t \boldsymbol{F}_t / M_p, \qquad (17)$$

and

$$\boldsymbol{\Omega}_p^{n+1} = \boldsymbol{\Omega}_p^n + \delta_t \boldsymbol{T}_t / I_p. \qquad (18)$$

After each time step, the position of particle $\boldsymbol{x}_p$ is updated by integrating the velocity with the following scheme:

$$\boldsymbol{x}_p^{n+1} = \boldsymbol{x}_p^n + \boldsymbol{u}_p^n \delta_t + \frac{1}{2}\delta_t^2 \boldsymbol{F}_t / M_p, \qquad (19)$$

### 2.3. Particle–particle and particle–wall interactions

If a massive amount of particles exist in a container, particles regularly approach within one lattice unit of each other or the wall under certain circumstances. When no fluid nodes exist for implementing the momentum exchange, the above force calculation will break down. In addition, the particles can interpenetrate each other or the wall in numerical simulations since the distances between them can become very small if no precautions are adopted. It is also noted that numerical errors may lead to such overlap in numerical calculations. In order to avoid those unphysical phenomena, we can introduce some short-range repulsive forces when the gap of the particle–particle or the particle–wall is less than a given threshold. In this work, we adopt the collision model proposed by Wan and Turek [39]. For the particle–particle collisions, the repulsive force is given by

$$\boldsymbol{F}_{i,j}^P = \begin{cases} 0, & d_{i,j} > R_i + R_j + \xi, \\ \frac{1}{\varepsilon_p'}(\boldsymbol{X}_i - \boldsymbol{X}_j)(R_i + R_j - d_{i,j}), & d_{i,j} \leqslant R_i + R_j, \\ \frac{1}{\varepsilon_P}(\boldsymbol{X}_i - \boldsymbol{X}_j)(R_i + R_j + \xi - d_{i,j})^2, & R_i + R_j \leqslant d_{i,j} \leqslant R_i + R_j + \xi, \end{cases} \qquad (20)$$

where $R_i$ and $R_j$ are the radii of the $i$th and $j$th particles, $\boldsymbol{X}_i$ and $\boldsymbol{X}_j$ are their centers, $d_{i,j} = |\boldsymbol{X}_i - \boldsymbol{X}_j|$ is the distance between the centers, $\xi$ is the threshold which is set to be one lattice spacing in the present work, $\varepsilon_p'$ and $\varepsilon_P$ are two small positive stiffness parameters for particle–particle collisions and they are set to be $1.0 \times 10^{-7}$ in our simulations. Similarly, for the particle–wall collisions, the repulsive force is given by

$$\boldsymbol{F}_i^W = \begin{cases} 0, & d_i' > 2R_i + \xi, \\ \frac{1}{\varepsilon_W'}(\boldsymbol{X}_i - \boldsymbol{X}_i')(2R_i - d_i'), & d_i' \leqslant 2R_i, \\ \frac{1}{\varepsilon_W}(\boldsymbol{X}_i - \boldsymbol{X}_i')(2R_i + \xi - d_i')^2, & 2R_i \leqslant d_i' \leqslant 2R_i + \xi, \end{cases} \qquad (21)$$

where $\boldsymbol{X}_i'$ is the coordinate vector of the center of the nearest imaginary particle located on the boundary and $d_i' = |\boldsymbol{X}_i - \boldsymbol{X}_i'|$, $\varepsilon_W'$ and $\varepsilon_W$ are two stiffness parameters which are set to be $\varepsilon_W' = \varepsilon_p'/2$ and $\varepsilon_W = \varepsilon_P/2$ in the calculations. It should be pointed out that the supplementary force of particle collision, $\boldsymbol{F}_i^{col} = \boldsymbol{F}_{i,j}^P + \boldsymbol{F}_i^W$, is regarded as an external force added to the total force acting on the $i$-th particle.

## 3. Results and discussion

### 3.1. Code validation

In this section, we will validate our lattice Boltzmann code by comparison with the existing results for the sedimentation of circular particle in Newtonian fluid. The sedimentation of one circular particle in a channel is used as the first test problem. The computational domain is inside in a channel of $W = 2$ cm width and $H = 6$ cm height. A rigid circular particle with diameter $D = 0.25$ cm and density $\rho_p = 1.25$ g/cm$^3$ is initially located at $(1\text{ cm}, 4\text{ cm})$. The density and viscosity of the fluid are $\rho_f = 1.0$ g/cm$^3$ and $\mu = 0.1$ g/(cm s). At time $t = 0$, the fluid and particle are at rest. Under the gravity (the accelerating velocity $g = 980$ cm/s$^2$), the particle will be dragged to fall down. A uniform grid of $201 \times 601$ is used for the simulation. The values of the relaxation rates are given as follows: $s_0 = s_3 = s_5 = 0, s_1 = 1.1, s_2 = 1.25, s_7 = s_8 = 1/\tau$, and $s_4 = s_6 = 8(2 - 1/\tau)/(8 - 1/\tau)$. Fig. 1 show the time evolution of some quantities of the particle, including the vertical position and vertical velocity of the particle, Reynolds number $Re = \rho_p D \sqrt{u_p^2 + v_p^2}/\mu$, and translational kinetic energy $E_t = 0.5 M_p (u_p^2 + v_p^2)$, $u_p$ and $v_p$ denote the two components of particle velocity, $M_p$ is the mass of the particle. For comparison, other published results [39,40] for the same problem are also shown in the figure. Clearly, good agreement between these results can be observed. For the small difference seen in the figure after the particle touches the bottom, it is attributed to the difference in the numerical methods and the particle–wall treatments in the calculations.

The second test problem is the sedimentation of two circular particles in a channel, whose schematic is shown in Fig. 2. This problem has been extensively studied by many authors, and the conditions used here are the same as those presented by Jafari et al. [41] for comparison: The computation domain is $W \times H = 2$ cm $\times$ 8 cm; The density and viscosity of the fluid are $\rho_f = 1.0$ g/cm$^3$ and $\mu = 0.01$ g/(cm s), respectively. The particle density is $\rho_p = 1.01$ g/cm$^3$, and the diameter is $D = 0.2$ cm. Initially, the two particles are located at the channel centerline with a height of 7.2 cm and 6.8 cm, respectively. Both particles and flow are set to be rest at $t = 0$, and then the two particles commence their motion downward under the gravity force. In our simulations, the normal derivative of velocity is assumed to be zero at the outflow boundary, and no-slip boundary conditions are applied to the left and right walls. The non-equilibrium extrapolation scheme [42] is adopted here to treat the inlet and outlet boundary conditions. For convenience of description, the upper and lower particles are labeled as "Particle 1" (or P1) and "Particle 2" (or P2), respectively.

It is known that the two particles would undergo the DKT process when they move close to each other. Fig. 3(a)–(d) show the instantaneous vorticity at different times during the sedimentation. The simulation is conducted with a uniform grid of $250 \times 1000$ nodes and the relaxation time $\tau = 0.65$. From the figure, we can see that the DKT phenomenon is successfully reproduced. Before proceeding to comparison with previous numerical results, we investigate the grid effect on numerical results obtained by the present method. To this end, we also conducted another two simulations using $200 \times 800$ and $300 \times 1200$ grid meshes, and the instantaneous horizontal and vertical positions of the two particles with three different meshes are plotted in Fig. 4. As the grid resolution is refined, one can clearly observe from the figure that the results under the $250 \times 1000$ and $300 \times 1200$ grids are consistent with each other, which demonstrates the consistent grid convergence of our used method. Based on this, we will use 25 lattice units to represent the particle in the following simulations. In addition, we would like to point out that if the relaxation rates $s_4$ (and $s_6$) are not chosen according to Eq. (13), no grid-independent results can be obtained.

Fig. 4 also includes the results of Jafari et al. [41], which are computed by the LBM with a smoothed-profile method. As can be observed, the results of the two methods are in good agreement overall with each other. The tiny differences shown in the figure during tumbling and subsequent separation processes can be
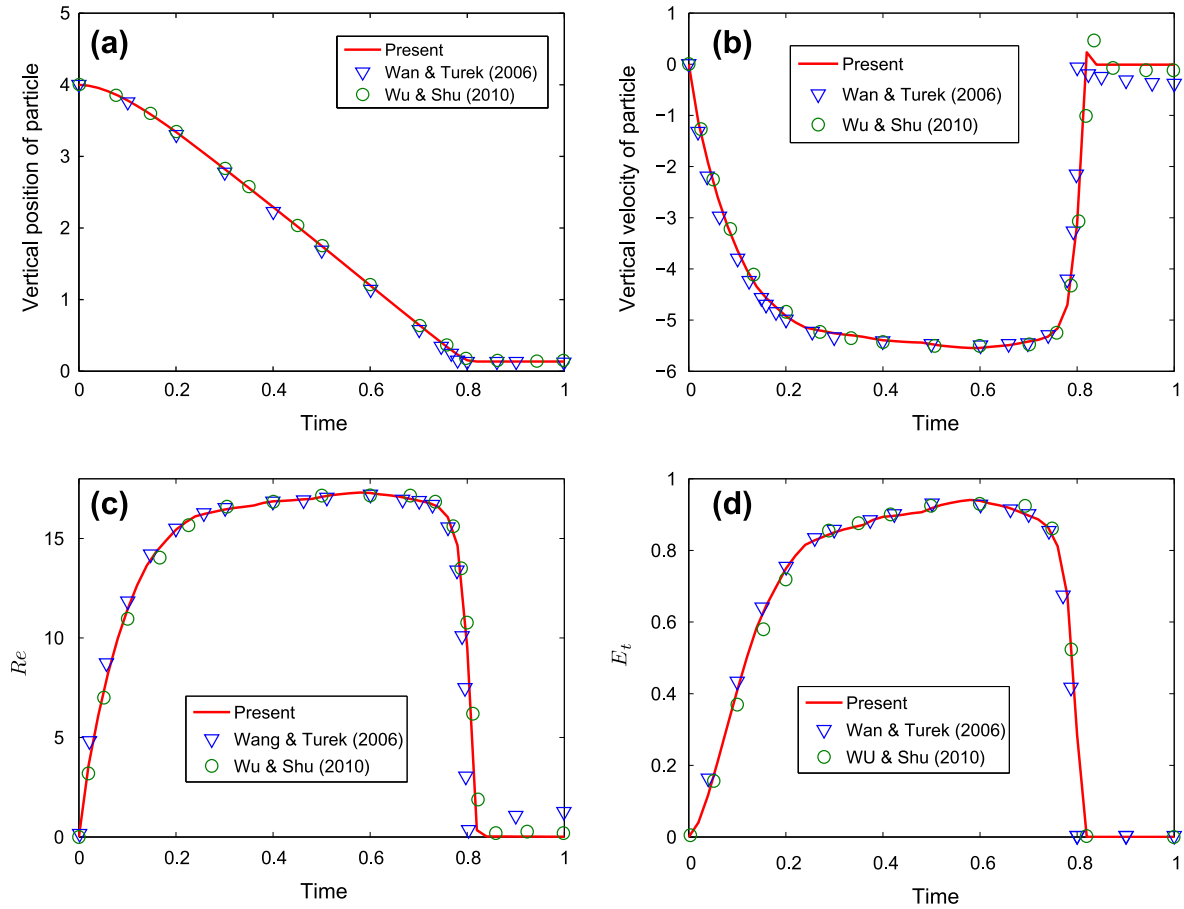
**Fig. 1.** Time history of the vertical position (*a*), vertical velocity (*b*), Reynolds number (*c*) and translational kinetic energy (*d*) of the particle during sedimentation.
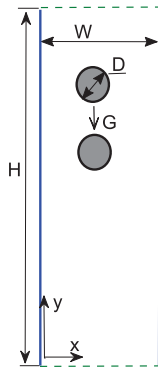


**Fig. 2.** Schematic of two circulate particles settling under gravity in an infinite channel.

attributed to the different particle–particle collision strategies in the present method and that in Ref. [41].

For better understanding of the DKT motion, we also measure the time development of three distances between two particles, i.e., the difference of transverse coordinates ($D_x$) and longitudinal coordinates ($D_y$) of the two particle centers, and the gap between the two surfaces $D_r = \sqrt{D_x^2 + D_y^2} - D$. As shown in Fig. 5, Particle 1 initially trails Particle 2 and a steady gap of about 0.2 cm between them keeps up for about $t = 0.7$ s. Thereafter, the trailing particle moves faster than the leading one, and they start to approach closer. This stage of motion is called "drafting". After this, the two particles almost touch each other at approximately
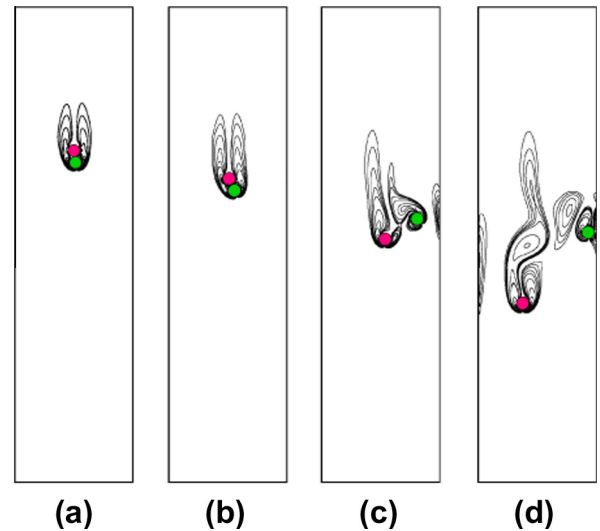


**Fig. 3.** Contours of vorticity at four time instants during sedimentation of two circular particles: (*a*) $t = 1.5$ s; (*b*) $t = 1.8$ s; (*c*) $t = 2.5$ s; (*d*) $t = 3.5$ s.

$t = 1.4$ s, which implies that they enter the "kissing" stage of the motion. At this time, the gap $D_r$ between the particles is approximately equal to zero (actually the gap is about one lattice spacing due to the collision model used). Following the kissing regime, the two particles start to slowly deviate from the channel center, and they fall together with decreasing $D_y$ until they completely tumble at time $t = 2.1$ s. Although each difference of the transverse and
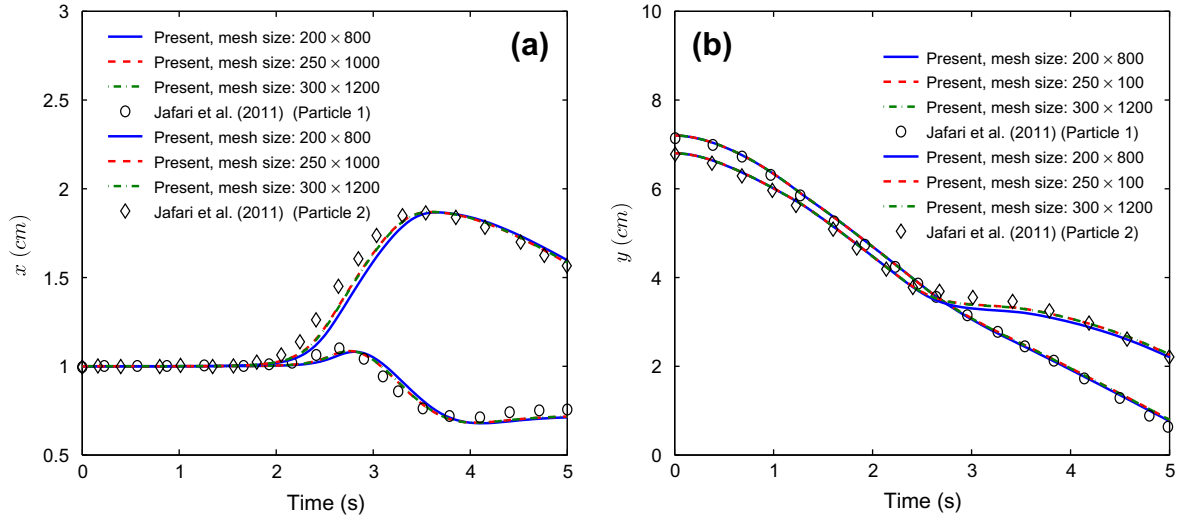
**Fig. 4.** Time history of two circular particles at three meshes during sedimentation: (*a*) transverse coordinates (*x*); (*b*) longitudinal coordinates (*y*) of two particles center. The numerical results by Jafari et al. [41] are also plotted for comparison.
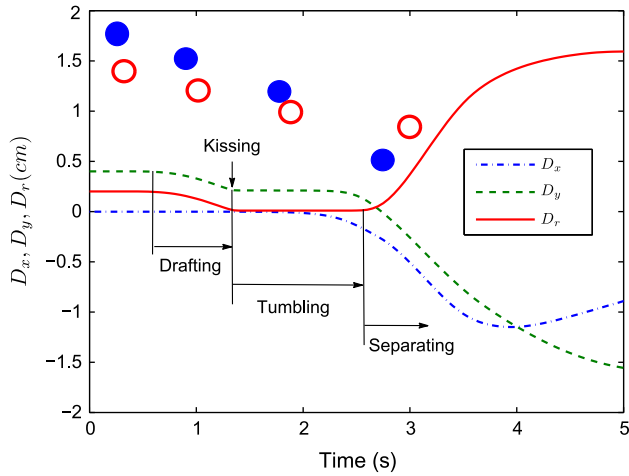


**Fig. 5.** Time history of the distances between two particles.

longitudinal positions between the two particles exhibits a relatively obvious variation during the "tumbling" stage, it is noted that the gap remains to be unchanged ($D_r \approx 0$), which implies the two particles are still in close contact with each other. Subsequent to this process, the two particles begin separating and throwing apart, and then distance themselves from each other. We would like to note that such similar phenomena were also observed in previous works [9,27]. In what follows, the three parameters ($D_x, D_y, D_r$) will be employed to analyze the interrelated motions between the two particles.

### 3.2. Sedimentation of two particles with different sizes

In this section, we investigate the hydrodynamic interactions of two circular particles with different sizes which sediment in an infinite channel. Particularly, the size effect of the particle pairs and the effect of initial longitudinal distance on their interactions will be investigated by comparison of the results for two identical particles in size. For two non-identical particles with different radii, two different configurations are considered with respect to the initial position, i.e., Case-1: the larger particle is located above the smaller particle, and Case-2: the smaller particle is above the larger one. Correspondingly, the case of two identical particles is

denoted by Case-0. In the following, we will make comparisons of the interactions between two particles in Case-0 and Case-1, as well as Case-0 and Case-2. In addition, comparisons of numerical results between Case-1 and Case-2 are also included.

To investigate the effect of particle size ratio, $\gamma = D_1/D_2$, where $D_1$ and $D_2$ are respectively the diameter of the larger particle and the smaller one, numerical simulations are performed by fixing the diameter of the larger particle at $D_1 = 0.2$ cm while varying the diameter of the smaller one. As demonstrated by Ladd [1,2] and Feng and Michaelides [43], accurate results can be achieved provided that the diameter of a particle is chosen to be greater than 20 lattice units. In our simulations, the smaller particle is covered by 25 lattice units while changing its diameter in our simulations. Unless otherwise specified, the other computational conditions are the same as those for two particles in the previous section.

To simulate an infinite channel, a moving computational domain is used during the simulations, where the upstream boundary is always $10D_1$ ahead of the particle, whereas the downstream boundary is $15D_1$ from the particle. The technique is briefly described as follows: If one of the two particles moves downward by one lattice unit, one layer of fluid nodes at the downstream side is removed from the grid system and one layer of lattice nodes is added to the upstream side. In addition, to avoid the particle moving out of the computational domain, the height of the computational domain is extended to be $H = 18$ cm. In our discussions, two kinds of Reynolds numbers based on the velocity and diameter of the particle will be used, i.e.,

Instantaneous Reynolds number $Re_a^i = \rho_f U_a D_i / \mu$

Terminal Reynolds number $Re_t^i = \rho_f U_t D_i / \mu$

where $D_i$ is the diameter of particle $i$, and $U_a$ and $U_t$ are the settling velocity and terminal velocity of the particle, respectively.

#### 3.2.1. Case 1. The larger particle above the smaller one

We now investigate the case of two different-sized particles, of which the larger one (P1) is initially set above the smaller one (P2). The diameter ratio $\gamma$ is first set to be 2 (i.e., $D_2 = 0.1$ cm). The two particles are released from rest with an initial gap of $D_h = 0.4$ cm. The locations are at heights of 15.0 cm and 14.6 cm in the channel, respectively.

Fig. 6 shows the positions and velocities of the two particles. For comparison, the results of two identical particles are also shown.
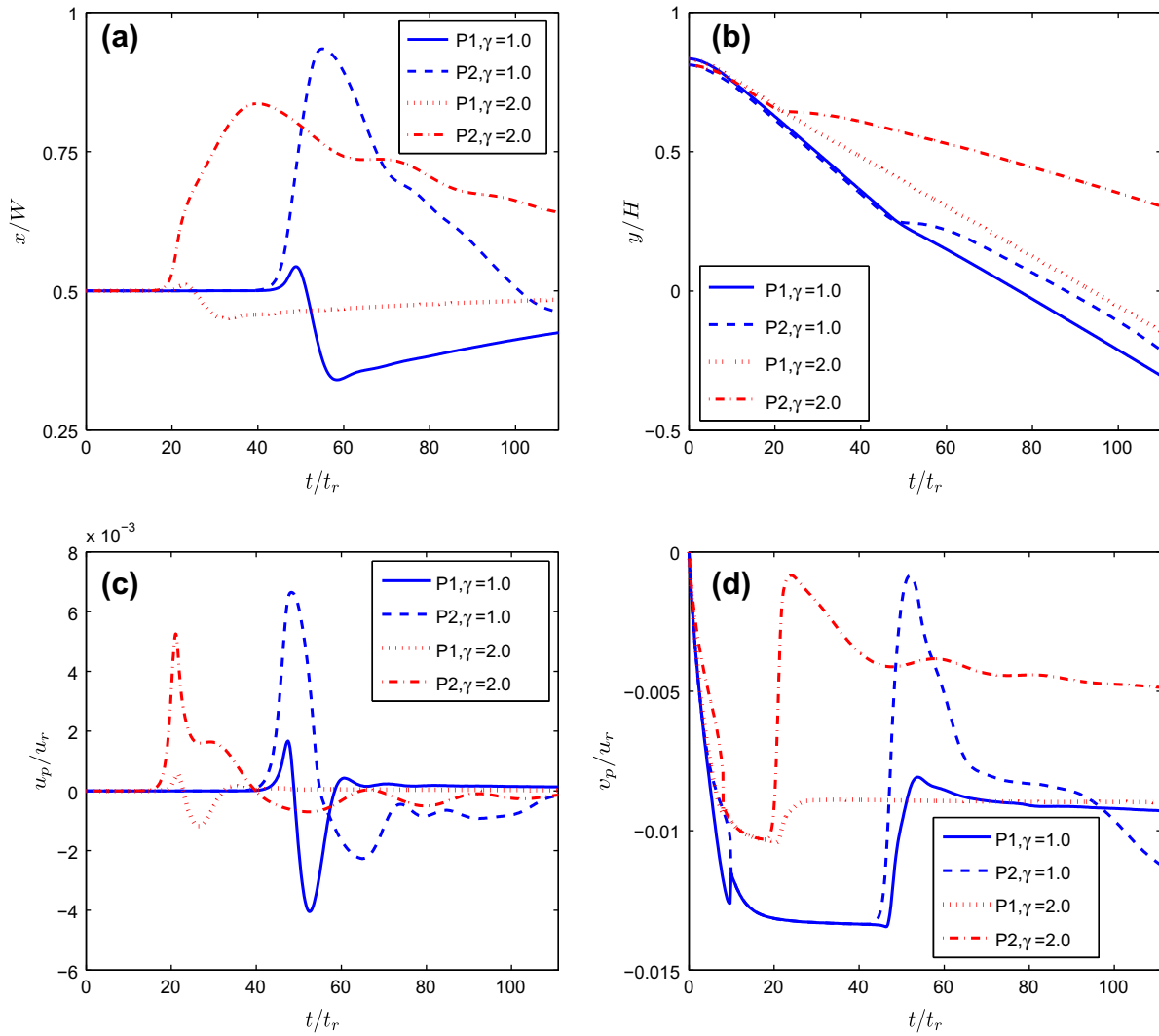
**Fig. 6.** Sedimentation of two circular particles. Particle position and velocity are compared for two different diameter ratios: $\gamma = 1.0$ and $\gamma = 2.0$. (a) Horizontal position, (b) vertical position, (c) transverse velocity, (d) longitudinal velocity.

The comparison of angular velocities of two particles are shown in Fig. 7. Henceforth, horizontal position will be normalized by $W$, vertical position normalized by $H$, time by $t_r$ with $t_r = \sqrt{H/g}$, velocity by $u_r$ with $u_r = \sqrt{Hg}$, angular velocity by $2\pi/t_r$, and distance between the two particles by $D_1$ in this work, unless otherwise specified. From Fig. 6(a) and (c) we can observe that after a time period of settling along the vertical direction, the particles with different sizes start deviating from their initial position to the right side at $t^* = t/t_r \approx 12.39$, while the two equal particles do not deviate towards right until $t^* \approx 27.3$. This implies that in the case of two non-identical particles P1 sediments more rapidly than P2 from the start. Notice that the two particles in these two cases have been in close contact with each other respectively at these two time points. Meanwhile, the two particles with different sizes begin to rotate in opposite directions. Specifically, in the case of two non-identical particles the initial leading one (P2) rotates with a higher angular velocity than the trailing one (P1) (see Fig. 7). After the leading particle changes to rotate in another direction, its angular velocity tends to approach zero together with the trailing particle. It is worth mentioning that the phenomenon for two equal-sized particles is similar to that observed by Qi [5] where the two particles are initial aligned at $x = 0.25W$. It can be also observed from Fig. 6(d) that at the early stage the larger
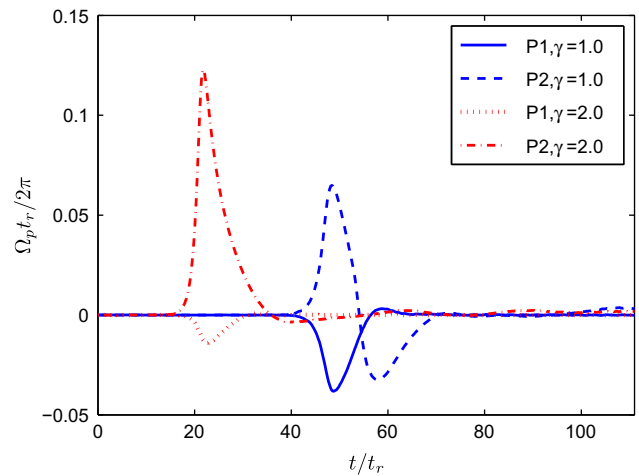


**Fig. 7.** The angular velocities as a function of time for two particles in Case-1.

particle moves faster than the smaller one, while in the case of two equal-sized particles the two particles move with almost the same velocity. Also, this indicates that when compared with the

case of two equal-size particles, the larger particle (the trailing particle) will be earlier to be influenced by the low pressure in the wake of the smaller particle (the leading particle). The drag which the larger particle experiences will decrease due to the wake effect behind the smaller one, and thus the larger particle can accelerate downward. As a result, the time when the two non-identical particles start to undergo the DKT process, especially the kissing state would be ahead of that for two identical particles, as clearly shown in Fig. 6(b) and (d).

To further support the above statements, we also investigated the fluid velocity field around the two particles. The velocity profiles around the two particles for the two cases at $t^* = 0.7379$ are shown in Fig. 8. As seen, a couple of symmetrical vortices in both the left and right side of each particle are formed in the case of $\gamma = 1.0$, while in the case of $\gamma = 2.0$ the magnitude of the vortex flow around the smaller particle is obviously much smaller than that around the larger one. This result further confirms that the sedimenting velocity of the bigger particle is larger than that of the smaller one. Furthermore, unlike the uniformly moving fluid in the gap of the two identical particles, the induced flow velocity between the two non-identical particles shows an obvious trend of

decreases along the vertical direction of sediment. This indicates that in the case of $\gamma = 2.0$, the moving fluid between the two particles is influenced by the wake of the leading particle stronger than that in the case of $\gamma = 1.0$. This phenomenon can also be evidenced from Figs. 9 and 10, where the pressure fields around the two particles and the pressure distribution along the center line of the leading particle (P2) in the vertical direction are shown. As can be seen, the pressure difference between the surface of two particles in the case of $\gamma = 1.0$ is larger than that in the case of of $\gamma = 2.0$. A further calculation shows that the pressure gradient in this region for the case of $\gamma = 1.0 \, (5.76 \times 10^{-2})$ is much higher than that for the case of $\gamma = 2.0 \, (1.21 \times 10^{-2})$. This result is also found to be hold until the two non-identical particles touch each other.

On the other hand, the results of Fig. 7 show that during the tumbling stage and even for a time period after separation, the angular velocity of the lager particle is significantly smaller than that of the smaller particle. In other words, the change of the angular velocity of the larger particle is less than the smaller particle, which can be attributed to the difference in mass (and thus inertia). After a few periods, they all tend to zero in spite of weak oscillations due to viscous effect.

During the tumbling stage and the subsequent separation from each other, as expected, the larger particle offsets laterally from the channel centerline much less than the smaller particle, which is revealed by the difference in the lateral velocity in Fig. 6(a) and (c). This indicates that the smaller particle experiences a very large repulsive force from the larger one. Subsequent to this, the two particles migrate towards the centerline of the channel. In contrast, the two particles in Case-0 oscillate with a higher amplitude about the centerline. Furthermore, it will be shown later that the two particles in Case-0 undergo the repeated DKT motion at later stage, and thus such cross-motion will take place more than once. At the time of kissing in both cases, from Fig. 6(a) and (c) we also note that the lateral motion of Particle 1 (P1) is closer to the channel centerline and changes more slightly than that of Particle 2 (P2) during the DKT process for the first time. This difference indicates that the trailing particle pushes the leading one aside when they touch each other. As P2 moves towards the wall and hits the wall, the repulsive force from the walls pushes it back to the centerline. In addition, it should be noticed that after tumbling the two particles will exchange their position in the vertical direction. Since then, as displayed in Fig. 6(b) and (d), in the case of two non-identical particles the vertical distance between them continues to increase
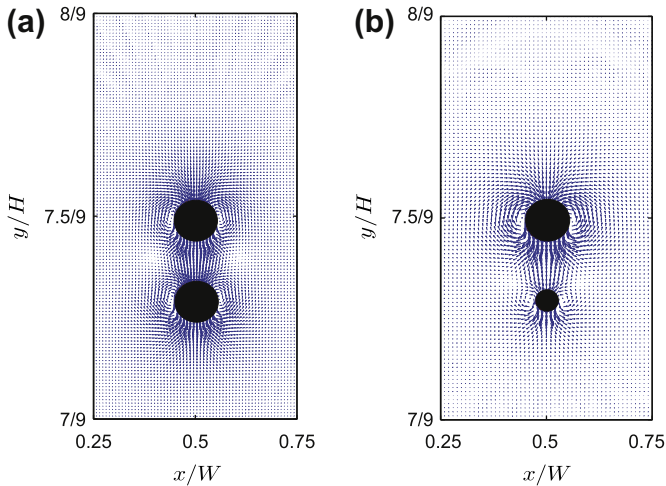


**Fig. 8.** The velocity field around the two particles for (a) $\gamma = 1.0$ and (b) $\gamma = 2.0$ at $t^* = 0.7379$.
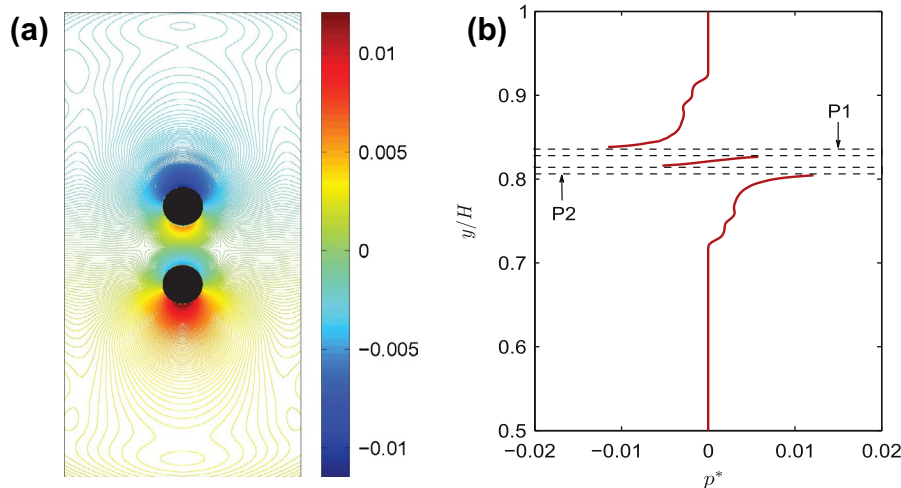


**Fig. 9.** (a) The pressure field around the two particles for $\gamma = 1.0$ at $t^* = 0.7379$. (b) Variations of the pressure along the center of the leading particle in the vertical direction for $\gamma = 1.0$ at $t^* = 0.7379$. In the figure plot, the pressure is taken to be the normalized value, that is, $p^* = (p - p_0)/(\rho_0 v_0^2)$. Here, $p$ and $p_0$ are the pressure and its average value in the flow field, and they are computed respectively through $p = c_s^2 \rho$ and $p_0 = c_s^2 \rho_0$. $\rho$ is the fluid density, and $\rho_0$ is the mean density averaged over the flow, and $v_0$ is the settling velocity of the trailing particle (P1). The dotted rectangular areas represent the regions of vertical positions occupied by the two particles.
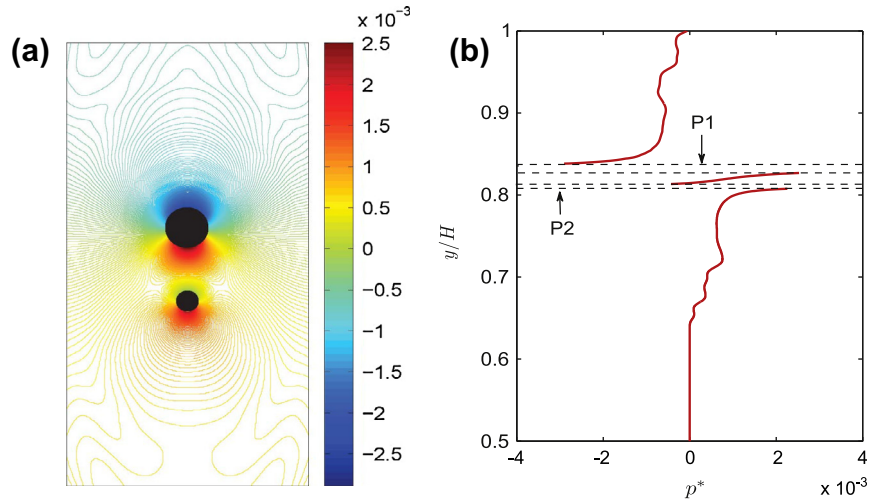
**Fig. 10.** (a) The pressure field around the two identical particles for $\gamma = 2.0$ at $t^* = 0.7379$. (b) Variations of the pressure along the center of the leading particle in the vertical direction for $\gamma = 2.0$ at $t^* = 0.7379$. In the figure plot, the pressure is taken to be the normalized value, that is, $p^* = (p - p_0)/(\rho_0 v_0^2)$. Here, $p$ and $p_0$ are the pressure and its average value in the flow field, and they are computed respectively through $p = c_s^2 \rho$ and $p_0 = c_s^2 \rho_0$. $\rho$ is the fluid density, and $\rho_0$ is the mean density averaged over the flow, and $v_0$ is the settling velocity of the trailing particle (the larger particle). The dotted rectangular areas represent the regions of vertical positions occupied by the two particles.
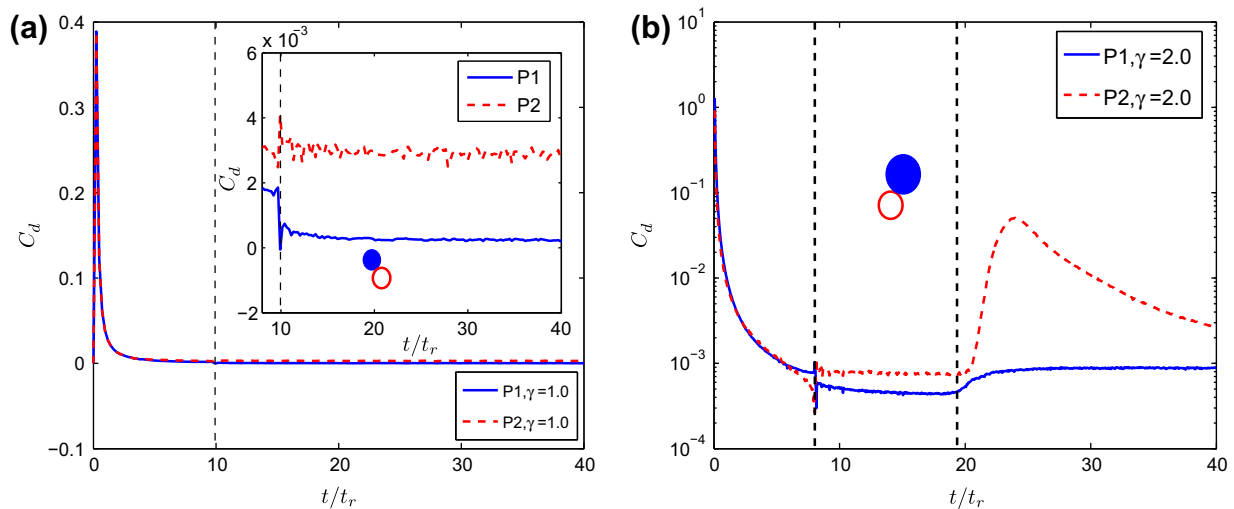


**Fig. 11.** Time development of drag coefficient with time at two cases: (a) $\gamma = 1.0$, (b) $\gamma = 2.0$. The vertical dash line of (a) corresponds to the time when two particles begin to touch each other, and the inset in (a) shows an enlargement of the figure since this time. The two dash lines of (b) indicate the time interval within which the vertical velocities of the two particles are approximately equal.

with time, and each particle eventually settles with a constant speed and reaches to a steady state. This clearly suggests that they will not perform the DKT process any more. However, for the case of two equal-sized particles the two particles will undergo the DKT process again (we will show this result later).

Also noteworthy from Fig. 6 is that there is a time duration in which the settling velocities of the two particles keep approximately equal from the kissing stage to the tumbling stage. Over this time intervals (see Fig. 6(d)), the settling velocities of two particles in Case-1 are smaller than those in Case-0, and also the time duration is much shorter in Case-1. Two effects are responsible for the difference. The first is the relative velocity of the two particles during the time duration, and the second is the length of the path over which the trailing particle travels. By measuring the difference in the transverse and longitudinal velocity between two particles, we find that the relative velocity of the two particles in Case-1 is indeed slightly larger than that of two particles in Case-0. At the same time, due to the size difference between the two

particles, the path along which the trailing particle rolls around the leading one in the tumbling process is much shorter for the case of two identical particles. In addition, when two particles contact with each other, the trailing particle is completely immersed in the wake region of the leading one. Due to the size difference of the leading particle between Case-0 and Case-1, the particle-induced flow between two particles in Case-1 drags the trailing particle downward more quickly. Taking these effects on the particle relative movement into account, the time duration for this case can be expected much shorter than that in Case-0.

The forces acting on the particles are also different in the two cases. Fig. 11(a) and (b) show the time history of drag coefficient in the vertical direction during $0 \leqslant t^* \leqslant 40$ respectively for Case-0 and Case-1. Here, the drag coefficient $C_d$ is measured from the following equation:

$$C_d = \frac{F_d}{\frac{1}{2}\rho_f U_p^2 D}, \tag{22}$$
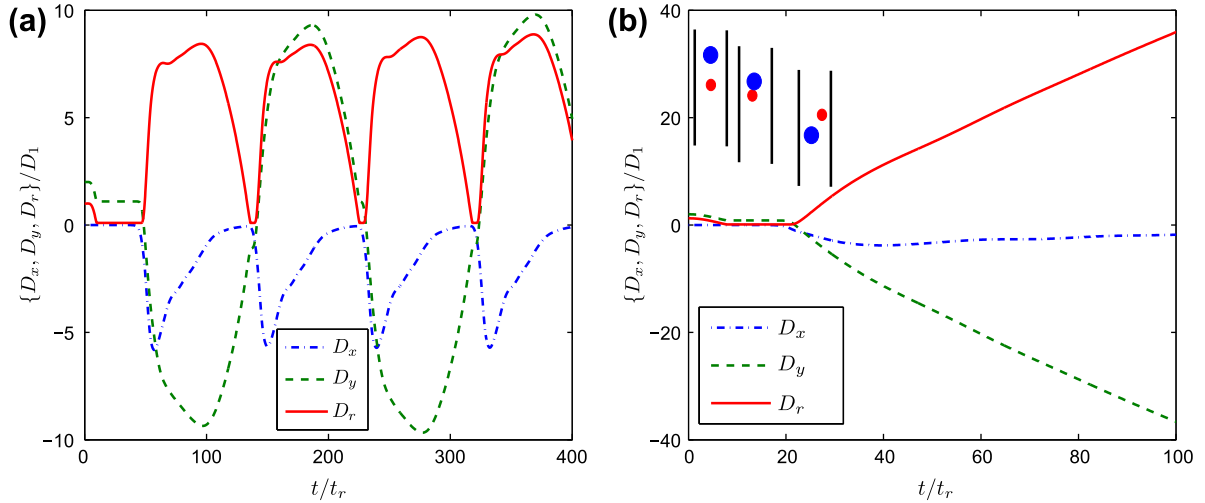
**Fig. 12.** The distances between two particles as a function of time for the case of (*a*) $\gamma = 1.0$, (*b*) $\gamma = 2.0$.

where $U_p$ is the settling velocity of the particle, and $F_d$ is the component of force acting on the particle in streamwise direction, which is computed according to the momentum-exchange method mentioned before. For both cases, it is observed that when the trailing particle moves to touch the leading one, the repulsive force between the two particles arises and leads to an obvious jump of the drag coefficients. After that, the drag coefficients of both particles reach to a steady value (indicated by the vertical dashed line in Fig. 11). In this time intervals, the corresponding Reynolds number $Re_a$, based on the settling velocity and the diameter of the particle, varies in the range of $30.7 \leqslant Re_a \leqslant 35.5$ for Case-0, and for Case-1 $Re_a$ falls in the range of $12.2 \leqslant Re_a \leqslant 13.67$ for P2, and $24.5 \leqslant Re_a \leqslant 27.5$ for P1. Particularly, when the two particles touch each other (indicated by the vertical dashed line in Fig. 11), the drag coefficients of the two particles in Case-1 are respectively lower than those in Case-0. This indicates that the two particles with different sizes are easier not only to touch but also to separate from each other than two identical particles.

In order to analyze the DKT process more clearly, we further examine the time development of the distances between two particles. Fig. 12 presents the three distances between the two particles as a function of time for the two cases. As discussed above, the first time of DKT process in Case-1 occurs earlier than that in Case-0. Similar to the results of Fig. 6(*b*) and (*d*), the time duration in Case-1 during which the two particles are in close contact is visibly shorter than that in Case-0. By measuring the time durations in Figs. 6(*d*) and 12, we find that they are consistent with each other. In addition, as pointed out above, it is clearly seen that the two particles in Case-0 interact by undergoing repeated DKT process [11], while the two particles in Case-1 do not appear to experience the DKT process any longer after the first time of the DKT process. When the two particles separate from each other, in Case-1 the smaller one falls significantly slower owing to the difference in the particle size. At this point, it is noticed that the larger particle have migrated below the smaller one (see Figs. 6(*b*) and 12(*b*)). As time elapses, the two particles migrate apart more from each other so that the smaller particle can no longer be sucked into the wake of the larger one, and the wake effect from the front particle on the latter one will fade. Thus, another DKT process would not be expected. In contrast, in the case of two equal-sized particles, the upper particle can shift into the wake of the lower one, where the pressure is low, after a period of sedimentation. Hence, the second DKT process and more will occur later on. Additionally, owing to the difference in the sedimenting velocity between two particles at $t^* > 96$, the gap between the larger and smaller particles increases linearly with time. At this time stage, the terminal particle Reynolds number $Re_t$ is 23.9 for the larger particle, and 6.73 for the smaller one.

*3.2.1.1. a. Effect of the initial distance.* From the above comparisons, it is revealed above that the larger particle sediments faster than the smaller one. Thus, one can infer that whatever the initial longitudinal distance ($D_h$) between two different-sized particles are set to be, the larger particle is bound to catch up with the smaller one originally in the lower position as time proceeds, and the DKT phenomenon will take place subsequently. Numerically, we conduct simulations with different $D_h$ to confirm this speculation. For example, even if $D_h/D_1 = 100$ the gap $D_r$ between two particles decreases with time until they touch each other, and they subsequently depart. In addition, it is found that $D_r$ continues to increase after the DKT process for each $D_h$. This indicates that the two particles can undergo the DKT process only once.

*3.2.1.2. b. Effect of diameter ratio.* We now consider the DKT phenomenon at different values of $\gamma$. As shown above, two modes are identified as $\gamma$ changes from 1 to 2: The two particles undergo the DKT process from repeatedly to just once. To investigate how these two modes change, we refined our simulations as $1 \leqslant \gamma \leqslant 2$. Fig. 13 shows the time history of the normalized gap
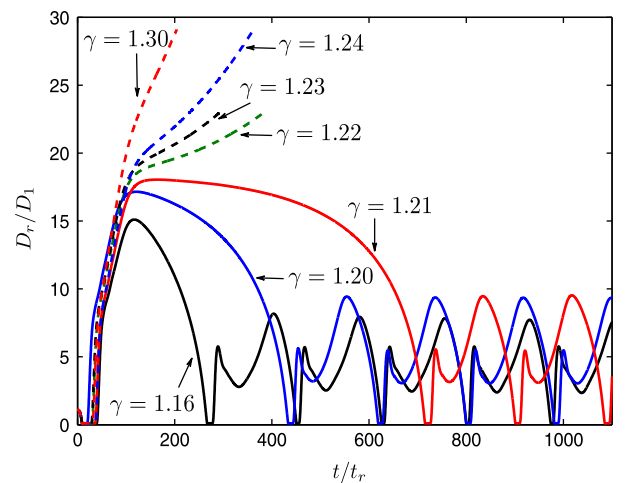


**Fig. 13.** Effect of variations of the diameter ratio in the range 1–2 on the DKT process.
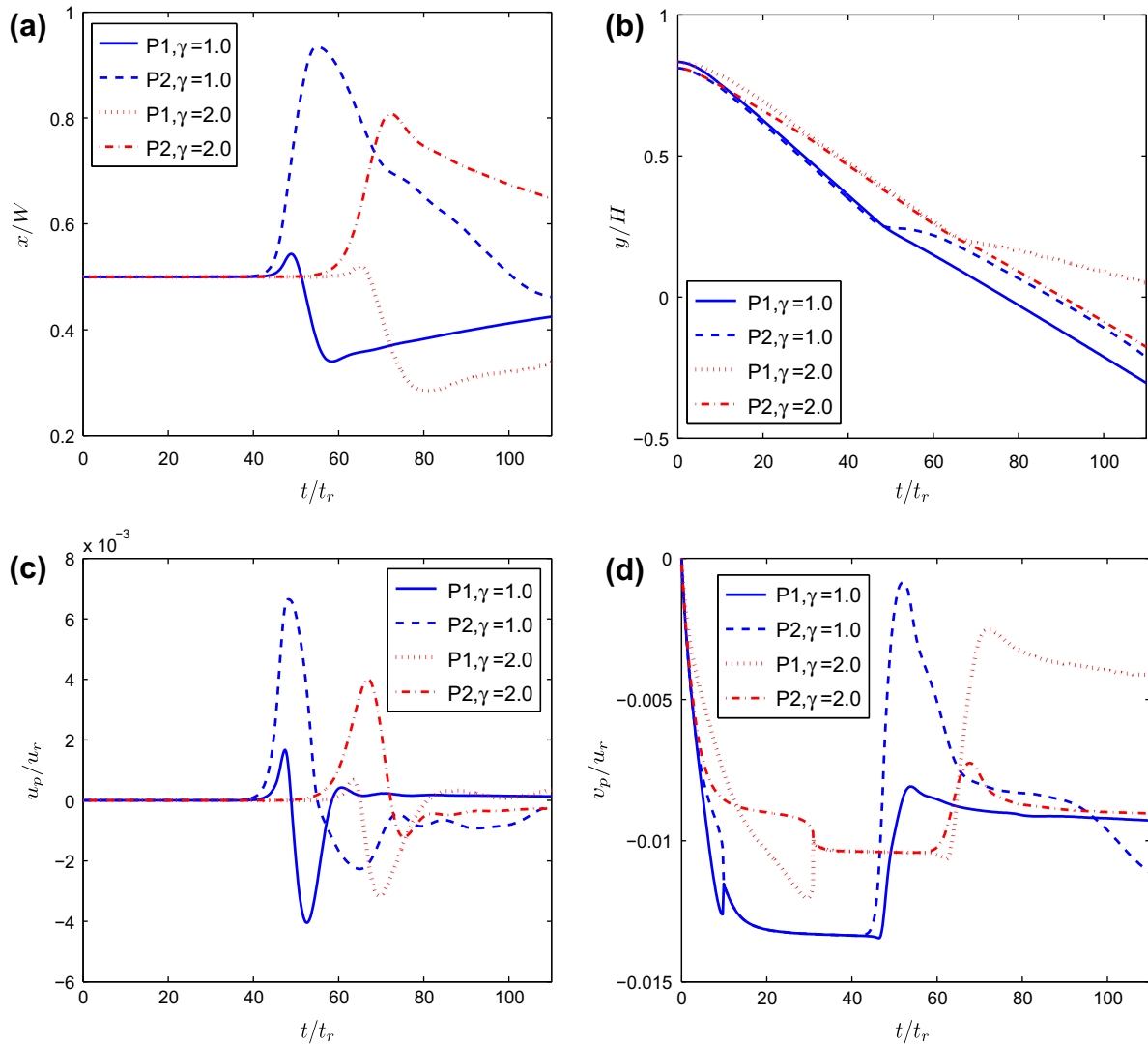
**Fig. 14.** Sedimentation of two circular particles. Particle position and velocity are compared for two different diameter ratios: $\gamma = 1.0$ and $\gamma = 2.0$. (a) Horizontal position, (b) Vertical position, (c) Transverse velocity, (d) Longitudinal velocity.

($D_r^* = D_r/D_1$) between two particles at different diameter ratios. For all the cases considered, $D_r^* = 0$ occurs at least once, which undoubtedly implies the occurrence of the DKT process. More importantly, it is observed that the two particles undergo repeated DKT process as $\gamma \leqslant 1.21$, while for $\gamma \geqslant 1.22$ the two particles separate from each other and the gap increases with time. This suggest that the critical value of $\gamma$ for the two patterns lies between 1.21 and 1.22. In addition, it is found that the repeated DKT process occurs more frequently with decreasing $\gamma$, which was also observed by Shao et al. [22] with some crude values of $\gamma$.

It is noted that as $\gamma > 2.0$, after the first time of DKT process the gap between two particles keeps increasing with time, which is in accord with the case of $\gamma = 2.0$.

### 3.2.2. Case 2. The smaller particle above the larger one

In this section, we consider the second case in which the smaller particle initially locates above the larger one. The computational conditions in the start state are the same as the above case except that the smaller particle is positioned at the height of $y = 15.0$ cm, and the larger particle at $y = 14.6$ cm. As before, $\gamma$ is first taken to be 2 in the following simulations.

Fig. 14 compares the particle motion and velocity versus time for Case-0 and Case-2. Regarding the lateral migration, the motions

of two particles in the two cases behave similarly. When compared with the corresponding results shown in Fig. 6(a) and (c), we observe that in Case-2 the larger particle migrates to the right side of the channel center more than the smaller particle, and the smaller particle experiences moving from the right to the left side of the centerline. Another difference is that the time at which the two particles deviates from their initial transverse position is at $t^* \approx 20.29$ in Case-2, while the deviation of two particles appears later in Case-0 and earlier Case-1. It is noted that the two particles are not in close contact with each other at this time (cf Fig. 14(b)). Also observed in Fig. 15 is that the two particles start to rotate in opposite directions. Thereafter, as the two particles migrate towards the lateral wall, the viscous forces reduces the transverse velocity of the two particles, and the particle–wall repulsive force pushes them backward the centerline.

On the other hand, as shown in Fig. 14(b) and (d), the settling velocities of two particles increase rapidly at initial times for both cases, while in Case-2 the smaller particle (the trailing particle) initially falls more slowly than the larger one (the leading particle) due to their difference in sizes, thus causing their longitudinal gap to increase with time. Subsequently, at $t^* \approx 12.9458$, the smaller particle begins to fall with a higher sedimenting velocity. As a result, the longitudinal gap turns to decrease until the two
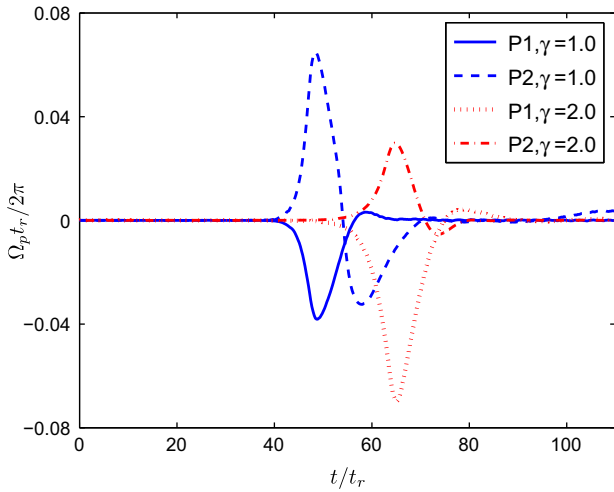
**Fig. 15.** Time development of angular velocities of two particles in Case-2.
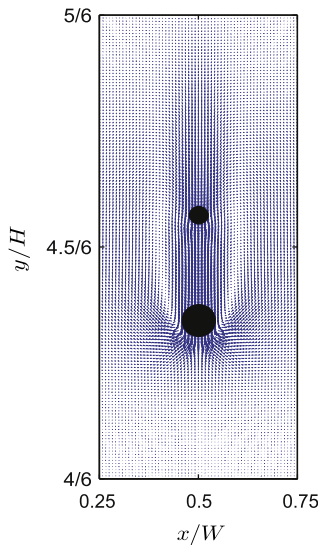


**Fig. 16.** Velocity field around the two particles of Case-2 at $t^* \approx 12.9458$.

particles touch each other. The reason for this behavior is that there is a strong suction effect on the smaller (trailing) particle due to the low pressure in the wake of the larger (leading) one, which causes the upper particle to fall more rapidly than the lower one. To confirm this speculation, we investigate the velocity field in the proximity region of the two particles at this time point. As shown in Fig. 16, the wake flow behind the larger particle extends beyond the smaller one, indicating that the smaller particle is strongly influenced by the wake of the larger one, and the smaller particle experiences less drag and thus it sediments with a higher velocity than the larger one. Fig. 17(a) and (b) show the pressure around the two particles and the pressure along the center of the larger particle in the vertical direction at $t^* = 12.9458$, respectively. At this time, it can be seen that the smaller particle has been sucked in the low-pressure region behind the larger one. Therefore, beyond this time the smaller particle will be accelerated. After evolving into the kissing stage, the two particles rotate more in the opposite direction as show in Fig. 15. Again, it is seen that the smaller particle rotates more rapidly than the larger one.

A common fact observed when the two particles "kiss" each other among the three cases is that the trailing particle is closer to the channel center than the leading particle (see Figs. 6(a) and

14(a)). One explanation accounting for this observation is that the trailing particle sediments faster than the leading one, and hence must push the leading particle aside to surpass it.

During the tumbling stage up to the subsequent separation from each other, the center of the smaller particle is always located above the larger one. This is quite different from those in the other two cases where the leading particle and the trailing particle exchange positions in the sedimentation direction (see Fig. 6(b)). In addition, it can be seen that the approximately equal value of the vertical velocities of the two particles (see Fig. 14(d)) is larger than that in the Case-1 in Fig. 6(d). This can be expected because in Case-2 the two particles move with a longer time period before they approach to each other. During this time interval, $Re_a$ for the smaller particle is $13.8 \pm 0.075$, and that for the larger particle is $27.6 \pm 0.150$. In addition, Fig. 18 shows the vertical drag coefficients of the two particles as a function of time. As seen from in the figure, the values of $C_d$ of the smaller particle is much smaller than those of the larger one. Thus, after this time duration, the sedimenting velocity of the smaller particle can keep higher value for a period of time although the two particles are still in close contact, as shown in Fig. 14(d).

Similar to the results in Fig. 6(d), as the two particles move farther away from each other, the interaction effects of two particles diminish and each particle falls with a steady velocity in the settling direction eventually (Fig. 14(d)). Thus, the DKT process will not be expected for the second time. During the two particles migrating towards the channel centerline at this stage, the magnitude of the angular velocity decreases with time, and oscillate about zero. Not surprisingly, the angular velocity of the smaller particle oscillates more significantly, as depicted in Fig. 15. Based on the basically unchanged settling velocity, $Re_t$ of the smaller particle is 6.78, and that of the larger one is 24.14. It can be found that the terminal particle Reynolds number of the two particles are almost the same in Case-1 and Case-2.

In order to more definitely resolve the behavior of the two particles during the DKT process, we show the distance between the two particles as a function of time in Fig. 19. As pointed out earlier, it is clear that in the initial time period of $0 \leqslant t^* \leqslant 12.9458$ (denoted by O–A) the gap $D_r$ (and $D_y$) between two particles increases with time, while the longitudinal distance $D_x$ remains unchanged without any deviation of transverse position of each particle. After this, the two particles start to interact by undergoing the characteristic behavior of the DKT process: drafting during $12.9458 < t^* < 30.8796$ (A–B), kissing and tumbling during $32.835 \leqslant t^* \leqslant 62.7185$ (B–C). After the tumbling stage, the gap $D_r$ (and $D_y$) increases further as time advances, suggesting that the two particles separate from each other and cannot perform the DKT process again. As also noted earlier, it can be clearly seen from Fig. 19 that $D_y$ is greater than zero throughout the whole time span. Notice that the smaller particle is initially located above the larger one in Case-2, which indicates that even when the DKT process is completed and the two particles become farther apart from each other, the smaller particle cannot always migrate to below the larger one.

*3.2.2.1. a. Effect of the initial distance.* We now investigate the effect of the initial longitudinal distance $D_h$ between two particles on their hydrodynamic interactions. In Fig. 20, the normalized gap $D_r^*$ between the two particles versus time at $\gamma = 2.0$ is presented for different normalized initial longitudinal distances. It can be seen that in each case $D_r^*$ increases during the initial time period. As $D_h/D_1 > 2.47$, a further increase of $D_r^*$ with time is observed because the wake of the larger particle imposes a smaller influence on the smaller trailing one. On the contrary, when $D_h/D_1 \leqslant 2.47$, $D_r^*$ first decreases to zero at a certain time, remains for a short period and then starts to increase. It is obvious that $D_r^*$ approaches to zero more rapidly as $D_h$ decreases. This can be explained by the fact that, as $D_h$
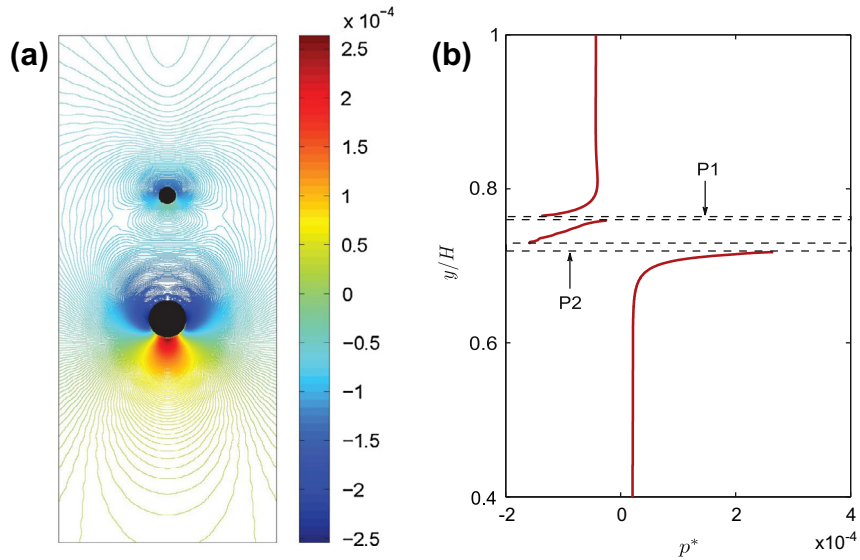
**Fig. 17.** (a) The pressure field around the two particles at $t^* \approx 12.9458$. (b) Variations of the pressure along the center of the larger particle in the vertical direction at $t^* \approx 12.9458$. The dotted rectangular areas represent the regions of vertical positions occupied by the two particles.
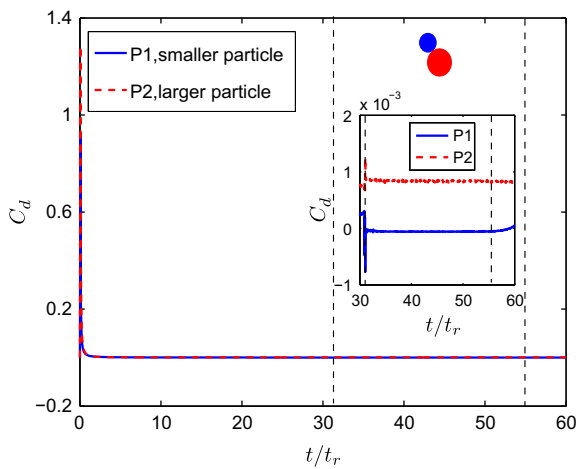


**Fig. 18.** Time history of drag coefficient with time in the vertical direction. The two dash lines indicate the time interval within which the vertical velocities of the two particles are approximately equal. The inset presents an enlargement of the results in the intervals defined by the dashed lines.
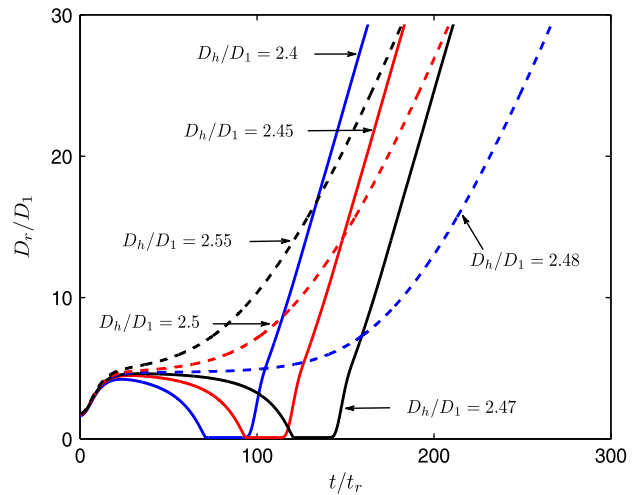


**Fig. 20.** Effect of initial longitudinal distance $D_h$ on the interaction of two particles at $\gamma = 2.0$.

is decreased, the smaller particle is pulled down more forcefully by the low pressure behind the large particle and so the catching time is shortened. Similar to the result in Fig. 19, after a time duration of staying at $D_r^* \approx 0$, $D_r^*$ increases with time rapidly which means that the two particles depart quickly. Therefore, we may conclude that for $D_h/D_1 \leqslant 2.47$ there would be only one DKT process taking place between the two particles.

*3.2.2.2. b. Effect of the diameter ratio.* The above results with regard to the effect of initial distance on the interactions between two different particles have demonstrated that the initial positions between the particles in the settling direction has strong influence on their interaction dynamics, such as the occurrence of the DKT process. Accordingly, we examine next how the diameter ratio influence the dynamic behavior of two particles, of which the smaller particle is placed above the larger one. To investigate the effect of diameter ratio, the normalized initial longitudinal distance is fixed to be $D_h/D_1 = 2$.

Note that the DKT process can take place once under the present position at $\gamma = 2.0$. We first pay our attention to the cases in



**Fig. 19.** Time evolution of distances between two particles.

which the diameter ratio is, as discussed earlier, greater than 2. In Fig. 21, the gap between two particles for different values of $\gamma$ is plotted as a function of time. As clearly shown, for $\gamma \leqslant 2.23$, after a short period of sedimentation, the gap $D_r^*$ between the two particles narrows to zero, and then increases rapidly after staying in zero for some time. In contrast, for $\gamma > 2.23$, $D_r^*$ continues to increase with time. This indicates that the value of $\gamma = 2.23$ is a critical value for the occurrence of the DKT process.

On the other hand, we may recall that two identical particles will interact in the fashion of repeated DKT process for $D_h/D_1 = 2$. With this in mind, we may further investigate the influence of $\gamma$ ranging from 2 to 1 on the repeating occurrence of the DKT process. The variations of $D_r^*$ versus time are plotted in Fig. 22 for different values of $\gamma$. As expected, in each case, there is a time duration of $D_r^* = 0$ which, in general, grows with increasing $\gamma$. The following development of $D_r^* = 0$ appears to be classified into two modes by the critical value of $\gamma = 1.27$: for $\gamma \leqslant 1.27$, the zero-value of $D_r^*$ undergoes repeatedly, while for $\gamma > 1.27$ $D_r^* = 0$ does not occur any more. From these results, we can see that repeated DKT process can take place when the diameter ratio

changes in the range $1 < \gamma \leqslant 1.27$, while the DKT process occurs only once as $1.27 < \gamma \leqslant 2$.

Overall, as the effect of the diameter ratio on the interactions of two particles is concerned, we can divide $\gamma$ into three regimes especially for the occurrence of the DKT process: first, the two particles will undergo repeated DKT process over the range of $1 < \gamma \leqslant 1.27$; second, as $1.27 < \gamma \leqslant 2.23$ the two particles will undergo the DKT process only once; third, the DKT process will never occur as $\gamma > 2.23$.

## 4. Concluding remarks

In this paper, we studied the DKT process of two sediment particles with a lattice Boltzmann equation method. Particularly, we considered three cases, namely, Case-0: two identical particles; Case-1: the larger particle is initially located above the smaller one; and Case-2: the smaller particle is initially above the larger one. We first validated the reliability of the numerical method by comparing with the existing results for the sedimentation of one and two identical circular particles in a two-dimensional channel. The influences of the initial longitudinal distance and diameter ratio on the interactions between two different-sized particles were carefully analyzed. Three kinds of distances between two particles were introduced to analyze the interactions. The main conclusions of the study are summarized as follows:

(1) In Case-1, the increase of the initial longitudinal distance between the two particles have no effect on the occurrence of the characteristic DKT process. This is due to the fact that the larger particle settles more quickly than the smaller one. The increase of the diameter ratio will shorten the time for the two particles to undergo the DKT process, while the decrease of diameter ratio can enhance the occurrence of the repeated DKT process. If the two particles undergo the DKT process only once, it is noteworthy that after the end of the DKT process they will migrate farther apart from each other as time proceeds, and each particle will eventually migrate in the longitudinal direction with a steady-state settling velocity while does not migrate in the transverse direction with a zero lateral velocity. Furthermore, during the DKT process, the two particles will exchange positions in the settling position.

(2) In Case-2, it is found that the gap between two particles increases at the initial time periods of movement due to the difference in the particle size. In case that the two particles can undergo the DKT process, the longitudinal position of the smaller particle is kept above the larger particle, which is different from the previous results about the DKT phenomenon in the published literatures. As expected, the increase of the initial longitudinal distance yields a negative effect on the occurrence of the DKT process. This is because the more the smaller particle is away from the lager one, the weaker it is influenced by the low pressure behind the larger particle. The results of the effect study of diameter ratio show that the two particles would undergo three transitions in the pattern of dynamics of interaction from repeated DKT process, one-off DKT process and continuous separation from each other.

Compared with Case-0, it is found that in the case of two nonidentical particles the time duration for which the two particles keep close together in the maiden DKT process is significantly shorter.

In addition to the particle size, density difference is a significant factor characterizing the particle–particle interactions. Moreover, the wall effect on the results need to be considered under different blockage ratios. Additionally, we would like to point out that the extension of the present work from two dimensions to three dimensions is relatively straightforward without much difficulty. In the future, we will conduct a comprehensive investigation on the dynamics of interactions between two particles within the three dimensions.
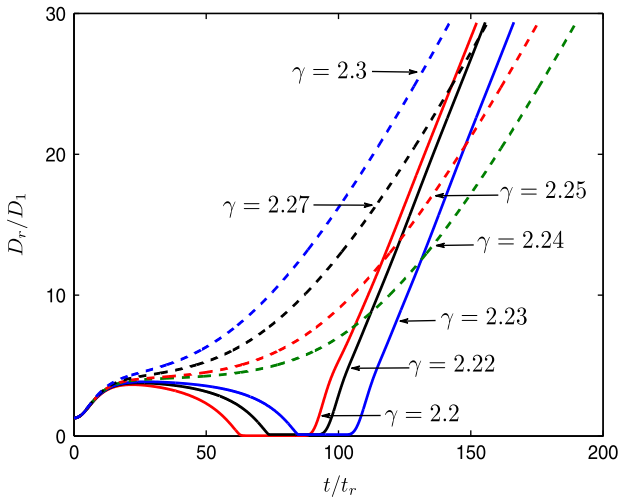


**Fig. 21.** Effect of variations of diameter ratio $\gamma$ in the region of $\gamma \geqslant 2$ on the interaction of two particles at $D_h/D_1 = 2$.
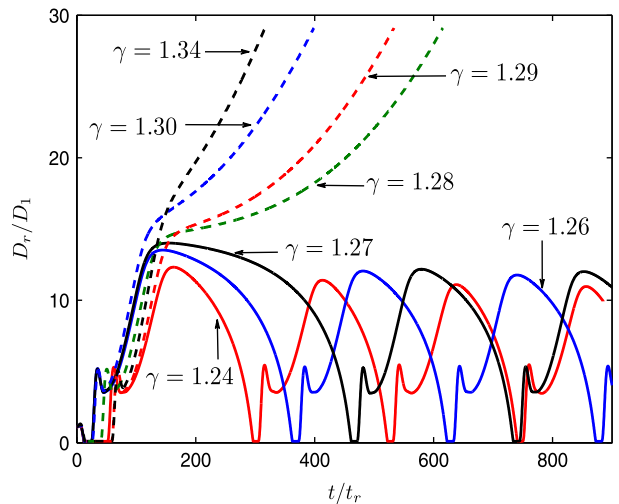


**Fig. 22.** Effect of variations of $\gamma$ in the interval $(1, 2)$ on the interaction of two particles at $D_h/D_1 = 2$.

## Acknowledgements

## References

[1] Ladd AJC. Numerical simulations of particulate suspensions via a discretized Boltzmann equation. Part I: Theoretical foundation. J Fluid Mech 1994;271:285–309.

[2] Ladd AJC. Numerical simulations of particulate suspensions via a discretized Boltzmann equation. Part II: Numerical results. J Fluid Mech 1994;271:311–39.

[3] Behrend O. Solid–fluid boundaries in particle suspension simulations via the lattice Boltzmann method. Phys Rev E 1995;52:1164–75.

[4] Aidun CK, Lu YN. Lattice Boltzmann simulation of solid particles suspended in fluid. J Stat Phys 1995;81:49–61.

[5] Qi DW. Lattice-Boltzmann simulations of particles in non-zero-Reynolds-number flows. J Fluid Mech 1999;385:41–62.

[6] Aidun CK, Lu YN, Ding EJ. Direct analysis of particulate suspensions with inertia using the discrete Boltzmann equation. J Fluid Mech 1998;373:287–311.

[7] Chen S, Doolen GD. Lattice Boltzmann method for fluid flows. Annu Rev Fluid Mech 1998;30:329–64.

[8] Ladd AJC, Verberg R. Lattice-Boltzmann simulation of particle–fluid suspensions. J Stat Phys 2001;104:1191–251.

[9] Feng ZG, Michaelides EE. The immersed boundary-lattice Boltzmann method for solving fluid-particles interaction problem. J Comput Phys 2004;195:602–28.

[10] Dupin MM, Halliday I, Care CM, Alboul L, Munn LL. Modeling the flow of dense suspensions of deformable particles in three dimensions. Phys Rev E 2007;75:66707.

[11] Fortes A, Joseph DD, Lundgren TS. Nonlinear mechanics of fluidization of beds of spherical particles. J Fluid Mech 1987;177:467–83.

[12] Sun R, Chwang AT. Interactions between two touching spherical particles in sedimentation. Phys Rev E 2007;76:046316.

[13] Rad SH, Najafi A. Hydrodynamic interactions of spherical particles in a fluid confined by a rough no-slip wall. Phys Rev E 2010;82:036605.

[14] Feng J, Hu HH, Joseph DD. Direct simulation of initial value problems for the motion of solid bodies in a Newtonian fluid. Part 1. Sedimentation. J Fluid Mech 1994;261:95–134.

[15] Ritz JB, Caltagirone JP. A numerical continuous model for the hydrodynamics of fluid particle systems. Int J Numer Meth Fluids 1999;30:1067–90.

[16] Patankar NA, Singh P, Joseph DD, Glowinski R, Pan TW. A new formulation of the distributed Lagrange multiplier/fictitious domain method for particulate flows. Int J Multiphase Flow 2000;26:1509–24.

[17] Patankar NA. A formulation for fast computations of rigid particulate flows. Center Turbul Res Ann Res Briefs 2001:185–96.

[18] Singh P, Hesla TI, Joseph DD. Distributed Lagrange multiplier method for particulate flows with collisions. Int J Multiphase Flow 2003;29:495–509.

[19] Feng YT, Han K, Owen DRJ. Combined three-dimensional lattice Boltzmann methods and discrete element method for modeling fluid? Cparticle interactions with experiment assessment. Int J Numer Methods Eng 2010;81:229–45.

[20] Macmeccan RM, Clausen JR, Neitzel GP, Aidun CK. Simulating deformable particle suspensions using a coupled lattice-Boltzmann and finite-element method. J Fluid Mech 2009;618:13–39.

[21] Mukundakrishnan K, Hu HH, Ayyaswamy PS. The dynamics of two spherical particles in a confined rotating flow: pedalling motion. J Fluid Mech 2008;599:169–204.

[22] Shao XM, Liu Y, Yu ZS. Interactions between two sedimenting particles with different sizes. Appl Math Mech-Engl 2005;26:407–14.

[23] Lallemand P, Luo LS. Theory of the lattice Boltzmann method: dispersion, dissipation, isotropy, Galilean invariance and stability. Phys Rev E 2001;61:6546–62.

[24] d'Humières D, Ginzburg I, Krafczyk M, Lallemand P, Luo LS. Multiple-relaxation-time lattice Boltzmann models in three-dimensions. Phil Trans R Soc Lond A 2002;360:437–51.

[25] Ginzburg I, d'Humières D. Multireflection boundary conditions for lattice Boltzmann models. Phys Rev E 2003;68:066614.

[26] d'Humières D. Generalized lattice-Boltzmann equations. In: AIAA Rarefied Gas Dynamics: Theory and Applications. Progress in Astronautics and Aeoronautics, vol. 159. New York: Academic Press; 1992. p. 450.

[27] Niu XD, Shu C, Chew YT, Peng Y. A momentum exchange-based immersed boundary-lattice Boltzmann method for simulating incompressible viscous flows. Phys Lett A 2006;354:173–82.

[28] Peng Y, Luo LS. A comparative study of immersed-boundary and interpolated bounce-back methods in LBE. Prog Comput Fluid Dynam 2008;8:156–67.

[29] Wang L, Guo ZL, Shi BC, Zheng CG. Evaluation of three lattice Boltzmann models for particulate flows. Commun Comput Phys 2013;13(4):1151–72.

[30] Yu D, Mei R, Luo L-S, Shyy W. Viscous flow computations with the method of lattice Boltzmann equation. Prog Aerosp Sci 2003;39:329–67.

[31] Yu D, Mei R, Shyy W. A unified boundary treatment in lattice Boltzmann method. AIAA J 2003;953:2003.

[32] Ginzburg I, Adler PM. Boundary flow condition analysis for the three-dimensional lattice Boltzmann model. J Phys II 1994;4:191–214.

[33] He X, Zou Q, Luo LS, Dembo M. Analytic solutions and analysis on non-slip boundary condition for the lattice Boltzmann BGK model. J Stat Phys 1997;87:115–36.

[34] Luo LS. Analytic solutions of linearized lattice Boltzmann equation. J Stat Phys 1997;88:913–26.

[35] Luo LS, Liao W, Chen X, Peng Y, Zhang W. Numerics of the lattice Boltzmann method: effects of collision models on the lattice Boltzmann simulations. Phys Rev E 2011;83:056710.

[36] Mei R, Yu DZ, Shyy W, Luo L-S. Force evaluation in the lattice Boltzmann method involving curved geometry. Phys Rev E 2002;65:041203.

[37] He X, Doolen G. Lattice Boltzmann method on curvilinear coordinates system: flow around a circular cylinder. J Comput Phys 1997;134:306–15.

[38] Filippova O, Hänel D. Grid refinement for lattice BGK models. J Comput Phys 1998;147:219–28.

[39] Wan D, Turek S. Direct numerical simulation of particulate flow via multigrid FEM techniques and the fictitious boundary method. Int J Numer Meth Fluids 2006;51:531–66.

[40] Wu J, Shu C. Particulate flow simulation via a boundary condition-enforced immersed boundary-lattice Boltzmann scheme. Commun Comput Phys 2010;7:793–812.

[41] Jafari S, Yamamoto R, Rahnama M. Lattice-Boltzmann method combined with smoothed-profile method for particulate suspensions. Phys Rev E 2011;83:026702.

[42] Guo ZL, Zheng CG, Shi BC. An extrapolation method for boundary conditions in lattice Boltzmann method. Phys Fluids 2007;14:2007–10.

[43] Feng ZG, Michaelides EE. Interparticle forces and lift on a particle attached to a solid boundary in suspension flow. Phys Fluids 2002;14:49–60.